Available online at www.sciencedirect.com
SCIENCE DIRECT®
Journal of Catalysis 229 (2005) 206–212
JOURNAL OF CATALYSIS
www.elsevier.com/locate/jcat

Enhanced catalytic activity of ceria nanorods from well-defined reactive crystal planes

Kebin Zhou, Xun Wang, Xiaoming Sun, Qing Peng, Yadong Li *

Department of Chemistry and the Key Laboratory of Atomic & Molecular Nanosciences (Ministry of Education, China), Tsinghua University, Beijing, 100084, P.R. China;
National Center for Nanoscience and Nanotechnology, Beijing, 100084, P.R. China

Received 15 September 2004; revised 28 October 2004; accepted 1 November 2004

Abstract

The crystal plane of ceria plays an essential role in determining its catalytic oxidation properties. In this study, single-crystalline CeO_2 nanorods with well-defined crystal planes have been synthesized by a facile solution-based hydrothermal method. HRTEM studies reveal that the predominantly exposed planes are the unusually reactive {001} and {110} in the CeO_2 nanorods rather than the stable {111} in the irregular nanoparticles. Consequently, it is demonstrated that the CeO_2 nanorods are more reactive for CO oxidation than their counterparts, irregular nanoparticles. The present results indicate that catalysts with well-defined reactive sites may be "designed" because of the recent development of morphology-controlled synthesis of nanostructured materials.

Keywords: CeO_2 nanorods; Well-defined; Crystal planes; CO oxidation

1. Introduction

Designing and synthesizing a highly reactive/selective catalyst has been an intriguing and challenging goal in heterogeneous catalysis [1–3]. So far high-surface-area inorganic oxides are of interest because they exhibit numerous edges and corners for adsorption and activation of reactants [4,5]. However, these materials, which are usually composed of assorted polycrystals with different exposed crystal planes, possess several kinds of active sites, which exhibit different reactivities and usually lower activity. On the other hand, catalysts with well-defined reactive crystal planes have been the focus of interest because they have desirable properties [6–10]. A typical case may be iron catalysts used for the synthesis of ammonia. It was observed that preferentially exposed {111} planes at the surface of iron are crucial to generating excellent activity [7,8]. For methanol oxidation, the Pt{111}/Ru electrode was found to be the best fuel-cell anode [9]. Recently, Choudary et al. reported that MgO hexagonal crystals exposing the most {100} planes were more active than nanocrystalline samples [10].

Therefore, a desirable goal for catalyst design and synthesis would be to decrease the less reactive crystal planes and increase the more reactive ones so as to optimize the desired structure of the active sites. However, this has turned out to be a very difficult task for most of the practical catalysts [1–3,6]. Although large single-crystal model catalysts are characteristic of these features, the surface area of the "effective" planes is very small and far from practical application. Morphology-controlled synthesis of nanostructured materials, such as single-crystalline one-dimensional (1D) nanomaterials (wires, rods, belts, and tubes), may present an opportunity for the synthesis of catalytic materials with such desirable features because these novel materials nucleate and grow in an epitaxial manner, exposing defined crystal planes [11–13]. Moreover, they are usually synthesized under unusual conditions, and some reactive crystal planes may be obtained.

* Corresponding author. Fax: (+86) 10-62788765.
E-mail address: ydli@tsinghua.edu.cn (Y. Li).

0021-9517/$ – see front matter
doi:10.1016/j.jcat.2004.11.004

Ceria (CeO_2) has been extensively investigated in heterogeneous catalysis [14–16], especially as an oxygen buffer in three-way catalysts [17]. For this application, reactive ceria is needed. Unfortunately, numbers of previous studies have shown that ceria nanoparticles predominantly expose their least reactive {111} planes, and the generation of more reactive planes with defined structures is very difficult by conventional methods [18–25]. Recently, through an easy solution-based hydrothermal method, we synthesized most of the rare earth compounds with 1D morphology [11]. This indicates that fabrication of 1D nanostructures of CeO_2 may also be possible. Here the hydrothermal method was successfully used to synthesize CeO_2 nanorods, which are well-defined single-crystalline 1D nanostructures. An enhanced catalytic activity has been found for CO oxidation over CeO_2 nanorods compared with CeO_2 nanoparticles with high specific surface area.

2. Experimental

2.1. Synthesis of CeO_2 nanorods and CeO_2 nanoparticles

CeO_2 nanorods can be synthesized by a solution-based hydrothermal method as follows. $Ce(NO_3)_3 \cdot 6H_2O$ (1.5 g) was dissolved in distilled water, and proper amounts of 10% NaOH solution were rapidly added with stirring at about 200 rpm. A light yellow precipitate of amorphous CeO_2 appeared. After about 15 min of stirring, all of the slurry (the volume was about 35 ml) was then transferred into a 50-ml autoclave, which was filled with deionized water up to 80% of the total volume (the final NaOH concentration in the autoclave is about 2 M), and heated at 100 °C under autogenous pressure for 10 h. The system was then allowed to cool to room temperature. The final product was collected by filtration, washed with deionized water to remove any possible ionic remnants, and then dried at 60 °C and calcined at 350 °C for 4 h. CeO_2 nanoparticles were prepared by a traditional precipitation method: $Ce(NO_3)_3 \cdot 6H_2O$ was dissolved in distilled water, and then the pH value of the solution was rapidly adjusted to 12 with 10% NaOH solution with stirring. The precipitate was filtrated, washed with deionized water, dried at 60 °C for 24 h, and then calcined at 350 °C for 4 h.

2.2. Catalytic activity evaluation

The catalytic activities for CO oxidation were evaluated in a fixed-bed quartz tubular reactor. The catalyst particles (0.2 g) were placed in the reactor. The reactant gases (1.0% CO, 16% O_2, balanced with nitrogen) went through the reactor at a rate of 100 ml/min. The composition of the gas exiting the reactor was monitored by gas chromatography.

2.3. Materials characterization

Powder XRD was performed with a Bruker D8 Advance X-ray diffractometer with monochromatized Cu-K_α radiation ($\lambda = 1.5418$ Å). The size and morphology of all of the materials were measured with a Hitachi H-800 transmission electron microscope and a JEOL JEM-2010F high-resolution transmission electron microscope. XPS measurements were conducted with a VG ESCA LAB 220 i-XL system with Al-K_α radiation under UHV (5×10^{-9} Pa), calibrated internally by carbon deposit C (1s) binding energy (BE) at 284.6 eV. The BET surface area of catalysts was measured by N_2 adsorption with the single-point method. Hydrogen temperature-programmed reduction (TPR) was conducted with a conventional apparatus equipped with a TCD detector. Before the TPR analysis, the samples were treated in pure oxygen at 450 °C for 45 min. A molecular sieve trap was placed before the detector to adsorb the water produced. TPR was performed by heating of the sample (50 mg) at 10 °C/min to 950 °C in a 5% H_2–N_2 mixture flowing at 40 ml/min.

3. Results and discussion

3.1. TEM, XRD, XPS, and BET analysis of CeO_2 nanorods and CeO_2 nanoparticles

The as-obtained CeO_2 nanorods were 100–300 nm in length and about 13–20 nm in diameter (Fig. 1(a)). On the other hand, the CeO_2 nanoparticles exhibit irregular shapes; their agglomeration can be observed (Fig. 1(b)), and the mean size is about 8 nm, as calculated from Scherrer's equation. Powder XRD analysis (Fig. 2) shows that both CeO_2 nanorods and nanoparticles can be indexed to the pure fluorite cubic structures (space group Fm3m (225)) with a lattice constant $a = 5.411$ Å (JCPDS 34-0394). XPS analysis reveals that only Ce^{4+} can be detected, and the surface composition and the chemical states of Ce are essentially the same for the two samples (the XPS patterns are not shown here). The BET surface area of the as-prepared CeO_2 nanorods is 50.1 m^2/g, and that of the CeO_2 nanoparticles is 62.4 m^2/g.

3.2. TPR analysis of CeO_2 nanorods and CeO_2 nanoparticles

Temperature-programmed reduction (TPR) by H_2 has been used extensively in the literature to characterize the surface and bulk oxygen reducibility of ceria materials. As suggested by Terribile et al. [4], the real redox property of CeO_2 can be measured indirectly by TPR followed by reoxidation. Therefore, we interrupted the first TPR run at 650 °C when the low-temperature reduction process was completed, then the samples were reoxidized with pure O_2 at 450 °C, and a second TPR run was performed.

The TPR results of the first runs (Fig. 3) showed that both CeO_2 nanoparticles and CeO_2 nanorods exhibited

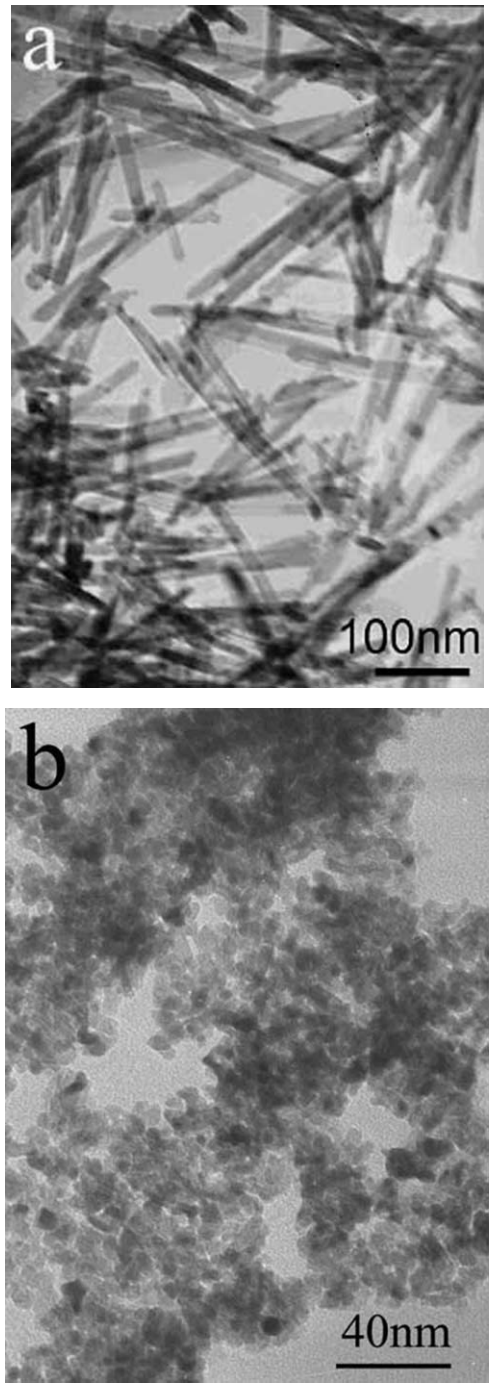

Fig. 1. TEM images of (a) CeO_2 nanorods and (b) CeO_2 nanoparticles.

a broad reduction profile centered around 500 °C and a high-temperature reduction peak above 700 °C. Quantitative evaluation of the low-temperature reduction peak (below 650 °C) indicated that hydrogen consumed by CeO_2 nanoparticles (153 $\mu mol_{H_2}/g$ of sample) was about three times larger than that consumed by CeO_2 nanorods (52 $\mu mol_{H_2}/g$ of sample), indicating a greater amount of surface oxygen on the CeO_2 nanoparticles.

However, the second TPR runs (Fig. 4) showed that almost 80% of the surface oxygen on the CeO_2 nanoparticles

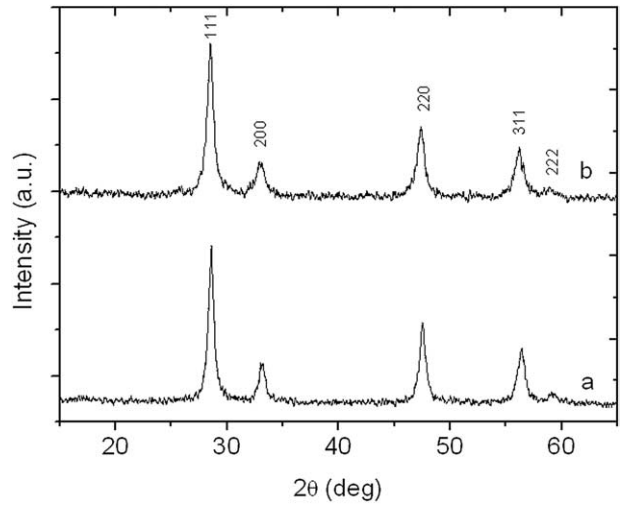

Fig. 2. XRD patterns of (a) CeO_2 nanoparticles and (b) CeO_2 nanorods.

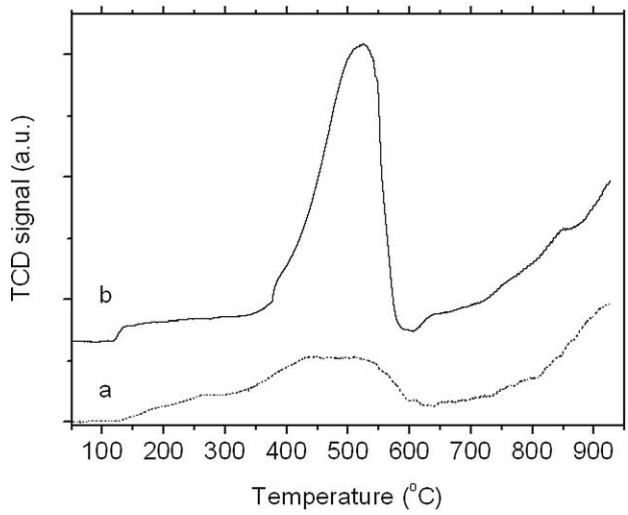

Fig. 3. Temperature-programmed reduction (TPR) profiles of the first runs. (a) CeO_2 nanorods and (b) CeO_2 nanoparticles.

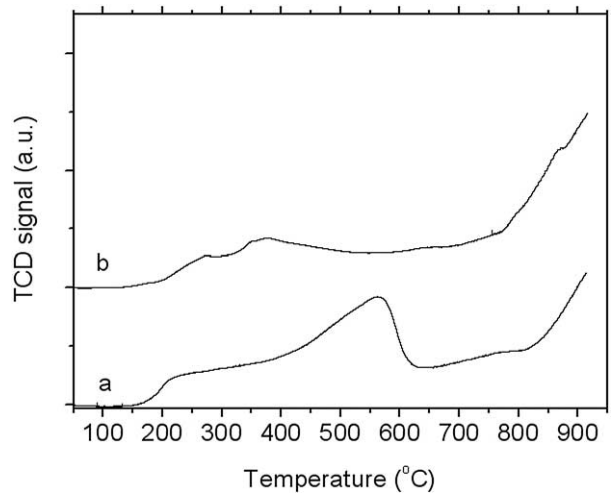

Fig. 4. Temperature-programmed reduction (TPR) profiles of the second runs. (a) CeO_2 nanorods and (b) CeO_2 nanoparticles.

was lost after cycling (the remnant was only 30.5 $\mu mol_{H_2}/g$). Meanwhile, promotion of Ce^{4+} reduction was observed on CeO_2 nanorods (60.4 $\mu mol_{H_2}/g$), revealing a stable facile Ce^{4+}/Ce^{3+} cycle. Loss of the low-temperature redox property of conventionally prepared CeO_2 nanoparticles was also observed by Terribile et al. [4]. The surface area of CeO_2 nanoparticles before the second TPR run was 52.6 m^2/g. Although the surface area was found to decrease by about 15.7%, this could not fully account for the severe loss of the redox property. A possible explanation for this may be the changes in ceria structure of some very fine clusters, as suggested by Putna and Cordatos et al. [26,27]. Simulated annealing calculations for small ceria clusters [27] demonstrate that the structure and reducibility of ionic clusters should depend strongly on the cluster size. The overall trend is for the larger particles to be more difficult to reduce. HRTEM analysis (in Section 3.4) in the present study shows that there were also some amorphous ceria clusters in the fresh nanoparticles; thus a higher reducibility was observed during the first TPR run. However, these fine ceria clusters might be very sensitive to the reducing atmosphere and structural changes might occur, resulting in lower reducibility during the second TPR run.

It is generally accepted that the low-temperature reduction process is a reduction of the surface oxygen species, which are catalytically active for CO oxidation [25]. Therefore, the relatively stable redox property of CeO_2 nanorods implies they may be more active than the traditional nanoparticles.

3.3. CO catalytic oxidation over CeO_2 nanorods and CeO_2 nanoparticles

CO oxidation is an important process in three-way catalysis. Measurements were made of the catalytic activity, the results are shown in Fig. 5. It is clear that CeO_2 nanorods are more active than CeO_2 nanoparticles. At 190 °C, the percentage CO conversion is 40% over CeO_2 nanorods and only 17% over nanoparticles; the corresponding rates of conversion of CO are 2.03 and 0.66 μmol/(g s), respectively. The rate of conversion over CeO_2 nanorods is therefore three times higher than that over nanoparticles.

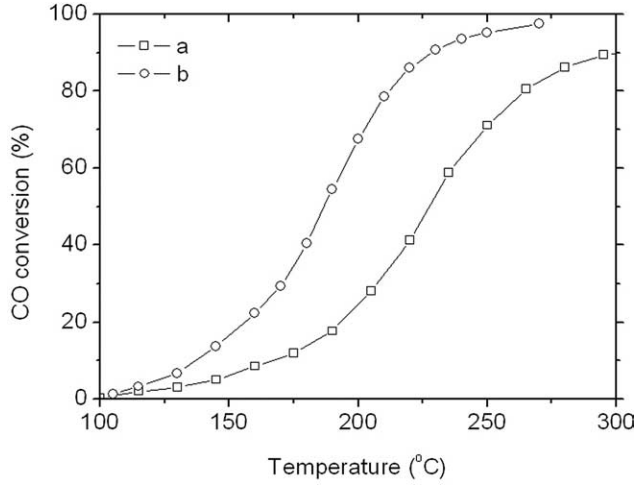

Fig. 5. Percentage conversion versus temperature plots for the oxidation of CO over (a) CeO_2 nanoparticles and (b) CeO_2 nanorods.

Table 1
Comparison of CO conversion over ceria catalysts

Sample	Calcination temperature (°C)	BET surface area (m^2/g^{-1})	T_{50} (°C)
CeO_2 nanoparticles	350	62.4	227
CeO_2 nanoparticles	600	54.3	285
CeO_2 nanorods	350	50.1	186
CeO_2 nanorods	600	48.5	190

We also observed a remarkable stability of the CeO_2 nanorods against calcination. Even after calcined in air at 600 °C for 4 h, the morphology of the nanorods remained unchanged and the activity decreased slightly. On the other hand, the particle size of irregular nanoparticles increased with calcination temperature and the catalytic performance decreased sharply. Table 1 summarizes the light-off temperatures T_{50}, corresponding to 50% conversion of CO. All of these data show the ceria nanorods are really more active than the "classical" ceria nanoparticles.

In general, high-surface-area nanocatalytic materials exhibiting numerous crystal faces, edges, and corners, which are conventionally considered active sites for the adsorption of reactants [4,5,28], should generate better catalytic performance. However, in the present study CeO_2 nanoparticles, with higher surface area and smaller particle size, are poorer catalysts, whereas CeO_2 nanorods, with lower surface area and larger diameter, are more active and demonstrate a stable redox property. These unusual results for these two ceria nanomaterials inspire us to hope that specific crystal planes are indeed a determining factor that will prove useful.

3.4. HRTEM analysis of CeO_2 nanorods and CeO_2 nanoparticles

It is well known that there are three low-index planes in the ceria fluorite cubic structure, namely the very stable and neutral {111} plane, the less stable {110} plane, and the higher-energy {001} plane [22]. Previous computer simulations predicted that the energy required to create oxygen vacancies on the planes was related to their stabilities. The stability of the {111} plane is greater than that of {001} or {110}, and thus it is inherently less reactive [19–21]. Recently, using a projector-augmented wave (PAW) method based on density-functional theory, Yang et al. [29] found that there are different adsorption features for CO on {111} and {110} planes. Whereas only weak adsorptions are found on the {111} plane, there are both weak and strong adsorptions on the {110} plane. If exposed planes with higher surface energy could be generated and stabilized, they could provide active sites for catalytic reactions.

Obviously, it may help to recall the morphology of these ceria materials. Figure 6(a) shows a HRTEM image of the CeO_2 nanoparticles. The dominant lattice fringes are from {111}, which are observed when the particles are oriented along the [110] direction. The particles show two types of shapes: one is the octahedral, enclosed by eight {111} planes, and the other is the truncated octahedral, enclosed by eight {111} and six {001} planes [22,23]. Obviously, the predominantly exposed planes are the {111} in the CeO_2 nanoparticles, with a small amount of {001} planes. Combined with previous studies [22,23], the structural models of these nanoparticles are drawn in Fig. 6(b).

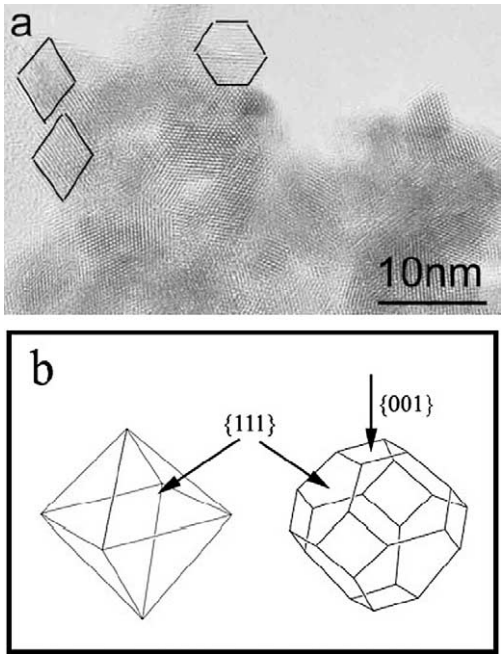

Fig. 6. (a) HRTEM image of the CeO_2 nanoparticles; (b) structural models of the octahedral and truncated octahedral shapes of CeO_2 nanoparticles.

In the case of the CeO_2 nanorods, cross-sectional views are necessary to identify all of the side planes. The cross-sectional TEM image of the CeO_2 nanorods is shown in Fig. 7(a). The cutting method used here is the well-established microtome technique widely used in the preparation of microscope samples, especially of biological specimens. The image clearly presents their rectangular cross section, indicating that each nanorod has four side surfaces. Figure 7(b) shows a HRTEM image of one typical CeO_2 nanorod. The upper right inset shows a selected area electron diffraction (SAED) pattern from the individual nanorod with a [001] zone axis. The inset on the lower right shows a magnified view of the selected area of the nanorod. Both insets indicate that the as-prepared CeO_2 nanorods are single-crystalline and the preferential growth direction is [110].

Figure 8(a) shows a two-dimensional crystal lattice image of one typical nanorod with a growth axis perpendicular to the electron beam. The SAED pattern (Fig. 8(b)) indicates the view direction is [001]. Based on the interplanar spacings, plane-intersecting angles, and the rectangular cross section, two sets of {002} planes and two {110} side planes of the rod can be identified. Another HRTEM image view along [1–10] is shown in Fig. 8 (c). Here one set of {001} planes and two {001} side planes of the rod are identified. On the basis of the above images, the four side planes of the nanorods are defined to be two {001} and two {110} planes. The structural models of these nanorods are drawn in Fig. 8(e).

The above HRTEM results reveal that CeO_2 nanorods predominantly expose the well-defined and less stable {001} and {110} planes, whereas in the CeO_2 nanoparticles the most stable {111} planes are predominantly exposed. And the activity data show that the ceria nanorods are more active than the “classical” ceria nanoparticles

In the course of the reaction, $–Ce^{4+}–O–$ is attacked and reduced by CO, and an oxygen vacancy can be created; then

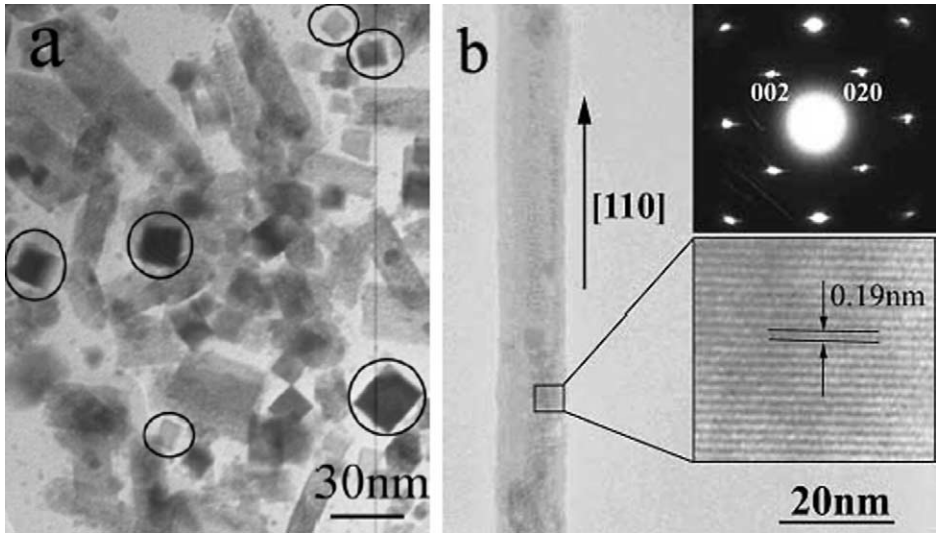

Fig. 7. (a) The cross-sectional TEM image of the CeO_2 nanorods; (b) HRTEM image of one typical CeO_2 nanorod. (The upper right inset shows a selected area electron diffraction (SAED) pattern from the nanorod; the lower inset shows a magnified view of the selected area of the nanorod.)

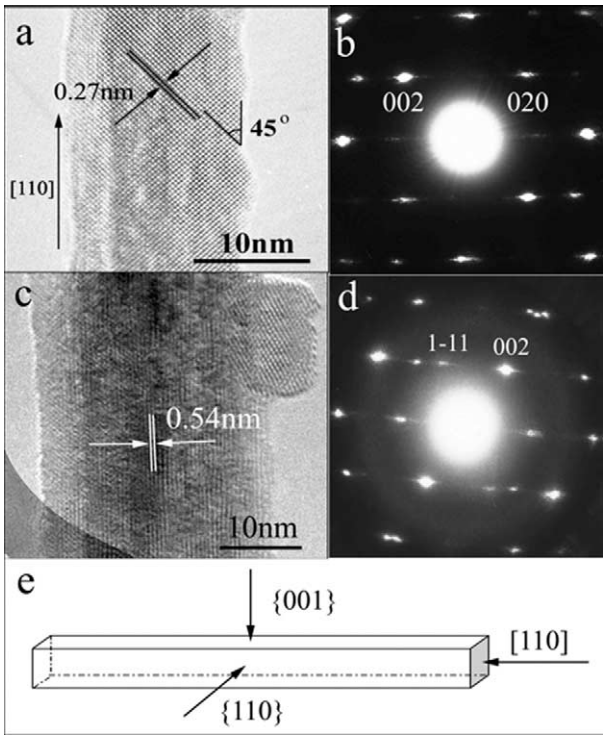

Fig. 8. (a) Magnified HRTEM of a typical nanorod view along [001]; (b) the SAED pattern of (a); (c) magnified HRTEM of a typical nanorod view along [110]; (d) the SAED pattern of (c); (e) the structural models of CeO_2 nanorods.

O_2 reacts with the surface to regenerate a surface oxygen atom. At an atomic level, this implies that the O_2 molecule dissociates at the vacancy site, with the formation of highly reactive atomic oxygen [30,31]. In the case of CeO_2 nanorods, the more reactive planes are exposed. Moreover, the stable redox property revealed by the TPR analysis indicates the reactive planes can be well protected. Thus a stable Ce^{4+}/Ce^{3+} cycle can easily be maintained to generate better catalytic performance during reaction. On the other hand, because of the predominant {111} planes, the real redox property of the CeO_2 nanoparticles is poorer than that of the nanorods, resulting in a lower activity. According to these results, a correlation can be drawn between the catalytic performance and the crystal planes: CeO_2 nanorods, with well-defined reactive planes ({001} and {110}), are more active than "classical" ceria nanoparticles with the {111} planes.

4. Conclusions

In summary, CeO_2 nanorods with well-defined reactive planes ({001} and {110}) can be synthesized by an easy solution-based hydrothermal method. These nanorods show higher CO oxidation activity than CeO_2 nanoparticles because of their more reactive planes. The present results suggest that catalysts may be "designed" rather than "prepared" because of the recent development of morphology-controlled synthesis of nanostructured materials. Through the control of a few critical synthesis parameters, nanomaterials with predictable morphologies, namely well-defined crystal planes, can be obtained, and the use of these materials as model catalysts in laboratory investigations as well as practical applications becomes possible.

Acknowledgments

This work was supported by the NSFC (50372030, 20025102, 20151001), the Foundation for the Authors of National Excellent Doctoral Dissertations of the People's Republic of China, and the State Key Project for Fundamental Research on Nanomaterials and Nanostructures (2003CB716901).

References

[1] A.T. Bell, Science 299 (2003) 1668–1691.
[2] H.H. Kung, M.C. Kung, Appl. Catal. A 246 (2003) 193–196.
[3] G.A. Somorjai, Y.G. Borodko, Catal. Lett. 76 (2001) 1–5.
[4] D. Terribile, A. Trovarelli, C. de Leitenburg, G. Dolcetti, Chem. Mater. 9 (1997) 2676–2678.
[5] M. Daturi, E. Finocchio, C. Binet, J.-C. Lavalley, F. Fally, V. Perrichon, H. Vidal, N. Hickey, J. Kašpar, J. Phys. Chem. B 104 (2000) 9186–9194.
[6] R. Schlögl, S.B. Abd Hamid, Angew. Chem. Int. Ed. 43 (2004) 1628–1637.
[7] G.A. Somorjai, in: Proceedings of the Robert A. Welch Foundation Conferences on Chemical Research, Houston, Texas, November 9–11, 1981, The surface science of heterogeneous catalysis, in: Heterogeneous Catalysis, vol. XXV, 1981, pp. 83–127.
[8] G. Ertl, in: Proceedings of the Robert A. Welch Foundation Conferences on Chemical Research, Houston, Texas, November 9–11, 1981, Primary steps in ammonia synthesis, in: Heterogeneous Catalysis, vol. XXV, 1981, pp. 179–207.
[9] W. Chrzanowski, A. Wieckowski, Langmuir 14 (1998) 1967–1970.
[10] B.M. Choudary, R.S. Mulukutla, K.J. Klabunde, J. Am. Chem. Soc. 125 (2003) 2020–2021.
[11] X. Wang, Y.D. Li, Angew. Chem. Int. Ed. 41 (2002) 4790–4793.
[12] X. Wang, Y.D. Li, J. Am. Chem. Soc. 124 (2002) 2880–2881.
[13] Y.N. Xia, P.D. Yang, Y.G. Sun, Y.Y. Wu, B. Marers, B. Gates, Y.D. Yin, F. Kim, H.Q. Yan, Adv. Mater. 15 (2003) 353–389.
[14] Q. Fu, H. Saltsburg, M. Flytzani-Stephanopoulos, Science 301 (2003) 935–938.
[15] G.A. Deluga, J.R. Salge, L.D. Schmidt, X.E. Verykios, Science 303 (2004) 993–997.
[16] S. Carrettin, P. Concepción, A. Corma, J.M.L. Nieto, V.F. Puntes, Angew. Chem. Int. Ed. 43 (2004) 2538–2540.
[17] A. Trovarelli, Catal. Rev. Sci. Eng. 38 (1996) 439–520, and references therein.
[18] T.X.T. Sayle, S.C. Parker, C.R.A. Catlow, Surf. Sci. 316 (1994) 329–336.
[19] D.C. Sayle, S.A. Maicaneanu, G.W. Watson, J. Am. Chem. Soc. 124 (2002) 11429–11439.
[20] B. Skårman, T. Nakayama, D. Grandjean, R.E. Benfield, E. Olsson, K. Niihara, L.R. Wallenberg, Chem. Mater. 14 (2002) 3686–3699.
[21] M. Lundberg, B. Skårman, L.R. Wallenberg, Micropor. Mesopor. Mater. 69 (2004) 187–195.
[22] F. Zhang, Q. Jin, S.-W. Chan, J. Appl. Phys. 95 (2004) 4319–4326.
[23] Z.L. Wang, X. Feng, J. Phys. Chem. B 107 (2003) 13563–13566.

[24] L. Dong, Y. Hu, F. Xu, D. Lu, B. Xu, Z. Hu, Yi. Chen, J. Phys. Chem. B 104 (2000) 78–85.
[25] H.C. Yao, Y.F. Yu Yao, J. Catal. 86 (1984) 254–265.
[26] E.S. Putna, J.M. Vohs, R.J. Gorte, J. Phys. Chem. 100 (1996) 17862–17865.
[27] H. Cordatos, D. Ford, R.J. Gorte, J. Phys. Chem. 100 (1996) 18128–18132.
[28] P.K. Stoimenov, V. Zaikovski, K.J. Klabunde, J. Am. Chem. Soc. 125 (2003) 12907–12913.
[29] Z. Yang, T.K. Woo, K. Hermansson, Chem. Phys. Lett. 396 (2004) 384–392.
[30] G. Pacchioni, ChemPhysChem 4 (2003) 1041–1047.
[31] P.G. Harrison, I.K. Ball, W. Azelee, W. Daniell, D. Goldfarb, Chem. Mater. 12 (2000) 3715–3725.